Step fluctuations on Ag(111) surfaces with C_{60}

C. Tao, T. J. Stasevich, T. L. Einstein, and E. D. Williams*
Department of Physics, University of Maryland, College Park, Maryland 20742-4111, USA
(Received 23 November 2005; revised manuscript received 21 February 2006; published 28 March 2006)

STM has been used to characterize fluctuation properties of segments of step edges partly covered by C_{60} on Ag(111) at room temperature. The distribution of C_{60} at step edges exhibits a step orientation dependence: Low-symmetry step edges are more favorable for C_{60} binding. The temporal correlation functions of step segments between C_{60}-covered step regions scale as a power law, with an average exponent of 0.23 ± 0.02, indicating that fluctuations of these "confined" steps are consistent with step-edge diffusion limited fluctuations. Parameters extracted from temporal correlation and autocorrelation analysis consistently indicate that close-packed steps have smaller fluctuation magnitude and higher step mobility than low-symmetry steps. The measured effective system sizes of step segments with different lengths show at most a weak step-length dependence. Fluctuation features thus yield the surprising conclusion that C_{60} molecules are not acting as pinning points that constrain mass transport along the step edges.

DOI: 10.1103/PhysRevB.73.125436 PACS number(s): 68.43.Jk, 68.65.−k, 68.37.Ef, 05.40.−a

I. INTRODUCTION

The challenge of nanoscience is to identify and exploit unique material properties that arise due to nanoscale size. Here we consider a novel possibility: The application of an immobile adsorbate to confine structural waves at nanometer length scales. Specifically, the system consists of monolayer-high steps (a boundary on a surface where the height changes by one atomic layer) on Ag(111). At room temperature, the step-edge fluctuates due to thermal motion of the Ag atoms along the edge of the step. The motion includes all the wavelengths accessible to the line within the correlation length.[1,2] The time constant τ_q for the evolution of each wavelength $\lambda = 2\pi/q$ is $\tau_q = k_B T/2\Gamma_h \tilde{\beta} q^4$, where $\tilde{\beta}$ is the step stiffness, related to the line tension, and Γ_h is the atomic mobility that underlies the step motion.[2] If step motion is "pinned," the maximum wavelength possible should be fixed at twice the distance between the pinning sites. In this work, we have investigated the physical nature of the size-limiting boundaries by using the preferential adsorption of C_{60} at step edges on Ag(111) to attempt physical confinement of step motion.

C_{60} on metal surfaces has been studied extensively.[3–6] At room temperature, on Ag(111) surfaces C_{60} films grow in a layer-by-layer manner with nucleation occurring at steps, followed by growth from steps onto both lower and upper terraces. C_{60} adlayers form a close-packed hexagonal structure of $2\sqrt{3} \times 2\sqrt{3}R30^\circ$ periodicity with respect to the substrate. We use C_{60} molecules at very low coverage ($<1\%$) to create regions of bare step edges of variable lengths. By directly measuring the temporal variation of the "pinned" step edges, we evaluate the effects of nanoscale structural confinement.

II. EXPERIMENTAL

The Ag(111) thin film preparation method has been described previously.[1] In an ultrahigh vacuum (UHV) chamber (base pressure $<10^{-10}$ Torr), Ag(111) thin films are sputtered and annealed. After several cycles, surfaces become atomically clean, as confirmed by both low-energy electron diffraction (LEED) and scanning tunneling microscope (STM). Under proper annealing conditions, step edges on the surface are well isolated from each other and have lengths up to 1 or 2 μm. C_{60} is evaporated from powder in a PBN crucible at deposition rate 0.01 ML/min, with the clean Ag(111) film held at room temperature. At low coverage, C_{60} molecules bind at the step edges and then nucleate small, close-packed islands, as shown in Fig. 1. At lower coverage, steps on the Ag(111) surfaces are only partly covered by C_{60}. Figures 2 and 3 are STM topography images, in which the bright dots along step edges indicate C_{60} molecules. In Fig. 3, the frizzy bare part of the step between C_{60}-covered regions clearly indicates fluctuation.[7,8] By controlling the annealing conditions and C_{60} coverage, the length distribution of the bare step region between C_{60}-covered regions can be readily changed.

For observation of step fluctuations, we use repeated STM scans across a fixed position at the step boundary, at the mid-point between the two ends of a bare segment of step-

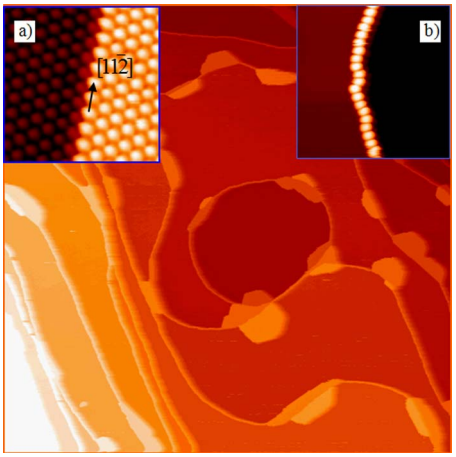

FIG. 1. (Color online) C_{60} chains and small islands along step edges on Ag(111) surface (400 nm × 400 nm, I=30 pA, V=−2.05 V. Figure 1(a), 10 nm × 10 nm. Figure 1(b), 15 nm × 15 nm).

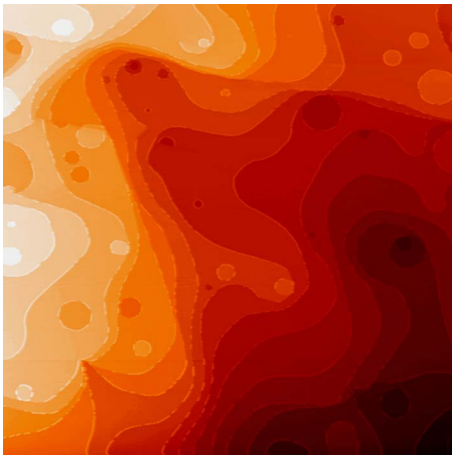

FIG. 2. (Color online) STM topography image of the Ag(111) surface with C_{60} molecules partly covering step edges (1000 nm $\times$ 1000 nm, I=110 pA, V=−1.54 V).

edge. The tunneling current is 0.10–0.12 nA, and sample bias 1.50 V. Under these tunneling conditions the tip-sample interactions can be negligible for Ag surfaces.[1,9] An example of a resulting pseudoimage is shown in Fig. 4. For all data in this paper, the time interval between scan lines is 51.2 ms, and the total measurement time is 102.4 s with 2000 line scans. This pseudoimage directly shows the magnitude of the edge fluctuations is up to ~0.6 nm. Fifteen to twenty sets of the step-edge position $x(t)$ data are measured for each step segment.

In order to extract the step-edge position $x(t)$, we flatten the image for the upper or lower terrace, and then identify the step point at which surface height is midway between the heights of the upper and lower terrace heights. The individual $x(t)$ data sets are used to calculate individual correlation and autocorrelation functions. The reported correlation and autocorrelation functions are averages of more than fifteen individual measurements.

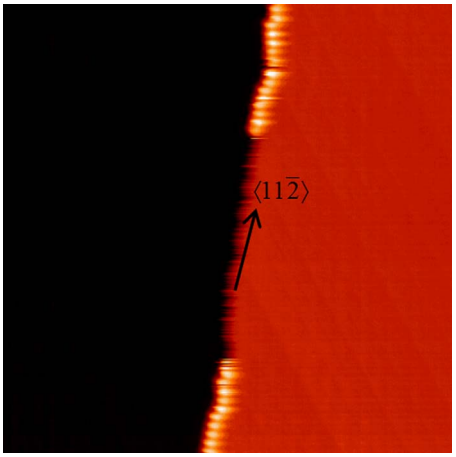

FIG. 3. (Color online) STM topography image of the monatomic steps on the Ag(111) surfaces partly covered by C_{60} molecules (40 nm $\times$ 40 nm, I=97 pA, V=−1.61 V).

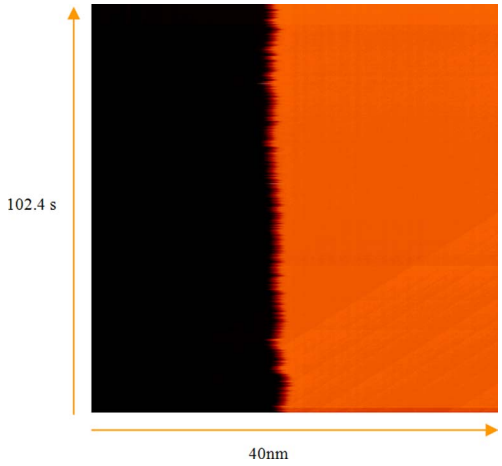

FIG. 4. (Color online) STM pseudoimage obtained by scanning the tip repeatedly over the middle point of the bare step edge. The line scan length is 40 nm, and a line-scan time is 0.0512 s. Total time is 102.4 s with 2000 lines. The tunneling conditions are I =97 pA, U=−1.61 V. The step orientation is along a close-packed direction.

III. RESULTS AND ANALYSIS

When C_{60} coverage is 4 to 5%, C_{60} molecules fully cover step edges and form small islands along step edges, as shown in Fig. 1. Figures 1(a) and 1(b) show, respectively, C_{60} islands that cross over step edges and C_{60} chains along step edges. Based on the atomic resolution STM images of the bare terraces or of C_{60} monolayer arrangement, the step orientation can be determined from the crystallographic symmetry. In Fig. 1(a), the underlying Ag step edge is along the "zigzag"-symmetry $\langle 11\bar{2}\rangle$ directions of the substrate, as indicated by the arrow. At lower coverage ($<1\%$), step edges on the Ag(111) surfaces are partly covered by C_{60}. On meandering step edges, C_{60} molecules are observed to avoid step edges along the close-packed $\langle 1\bar{1}0\rangle$ directions of the substrate and cover those parts deviating from the close-packed direction. To perform our measurement, we chose step segments with different lengths between adjoining C_{60} regions. Most of the larger step segments are along the close-packed directions of the substrate. However, shorter segments were found primarily at lower-symmetry orientations, as could be expected based on the C_{60} growth mode at low coverage.

In Fig. 3, the uncovered part of the step clearly reveals the presence of temporal fluctuations by the frizzy appearance. However, the C_{60} molecules appear motionless according to STM topography images (viz. the position is invariant from scan to scan), and look like pinning points on the step edges. In order to find out how the C_{60} molecules affect the step fluctuations, we measured steps with different bare lengths, from 10 nm to more than 100 nm.

The basic theory to describe the fluctuations of the step is Langevin analysis using the continuum step model.[2] Each degree of freedom of the step is assumed to diffuse towards lower energy with a speed proportional to the gradient of the energy, while random thermal noise tends to roughen the step edge. Previous studies have shown that step fluctuations on

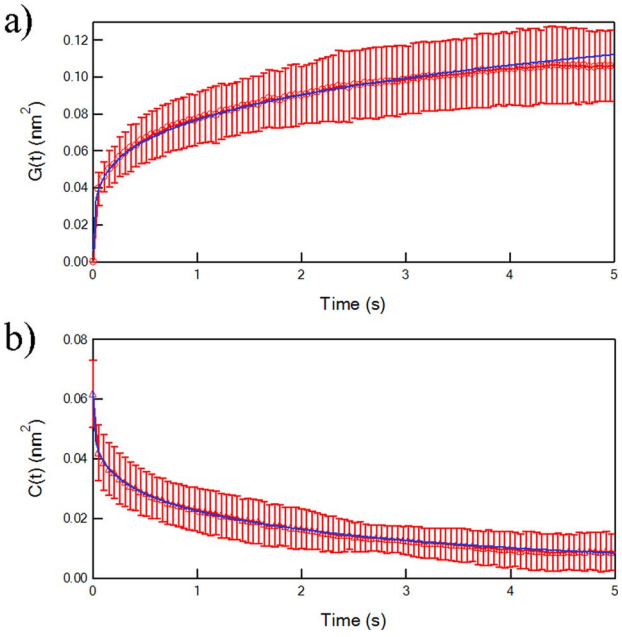

FIG. 5. (Color online) Typical $G(t)$ and $C(t)$ curves and fit curves. In both figures, solid lines (blue) are fitting curves using Eqs. (4) and (5). The best fit values are $C(0)=0.0627\pm0.0002$ nm^2, $\tau_c=11.26\pm0.10$ s, $G_0=0.0713\pm0.0005$ nm^2. The error bars shown are the standard deviation of the average over 12 sets of $x(t)$ data, all measured on the same step segment. This step segment is 51 nm, and orientated 5° deviating from close-packed direction.

bare Ag(111) surfaces are governed by step-edge diffusion.[1,9,10] Since atoms can only hop from one site to another on the step edge, the thermal noise is correlated. For this case, the Langevin equation governing step edge displacements is:

$$\frac{\partial x(y,t)}{\partial t} = -\frac{\Gamma_h \tilde{\beta}}{k_B T}\frac{\partial x^4(y,t)}{\partial y^4} + \eta(y,t), \tag{1}$$

with $\eta(y,t)$ the thermal noise and $\langle \eta(y,t)\eta(y',t')\rangle = -2\Gamma_h \delta(t-t')\delta''(y-y')$, where the step mobility $\Gamma_h = a_\perp^2 a_\parallel^3/\tau_h$, and $a_\parallel$ ($a_\perp$) is the lattice constant parallel (perpendicular) to the step edge, and τ_h the hopping time. Alternative kinetic processes that can induce step motion are terrace diffusion and attachment/detachment at the step edge. These processes have different governing equations and correlation functions.

As described in the experimental section, from pseudoimages we can extract the temporal displacements of the step edge, which is the step-edge position $x(t)$. Then we can calculate the time correlation functions $G(t)$ and autocorrelation functions $C(t)$ defined by, respectively:

$$G(t) = \langle (x(t+t_0) - x(t_0))^2 \rangle_{t_0}, \tag{2}$$

$$C(t) = \langle [x(t+t_0) - \bar{x}][x(t_0) - \bar{x}] \rangle_{t_0}. \tag{3}$$

The results for a step with a bare length of 51.0 nm between C_{60} molecules are shown in Figs. 5(a) and 5(b). According to the above Langevin description of periphery-diffusion dynamics,[1,11–13] $G(t)$ and $C(t)$ can be expressed as follows:

$$G(t) = \left(\frac{2\Gamma\left(\frac{3}{4}\right)}{\pi}\right)\left(\frac{k_B T}{\tilde{\beta}}\right)^{\frac{3}{4}}(\Gamma_h t)^{\frac{1}{4}} = G_0 t^{\frac{1}{4}}, \tag{4}$$

$$C(t) = C(0)\left(\left(e^{\frac{t}{\tau_c}}\right) - \Gamma\left(\frac{3}{4}, \frac{t}{\tau_c}\right)\left(\frac{t}{\tau_c}\right)^{\frac{1}{4}}\right), \tag{5}$$

$$C(0) = \frac{k_B T L}{2\pi^2 \tilde{\beta}}, \tag{6}$$

$$\tau_c = \left(\frac{L}{2\pi}\right)^4 \frac{k_B T}{\Gamma_h \tilde{\beta}}, \tag{7}$$

where Γ is the gamma function, τ_c the correlation time, and L is the system size, which is also often identified as the correlation length l_{corr} over which correlated motion can be observed. A synopsis of the parameters and symbols used in this discussion is presented in Table I. For alternative physical mechanisms, the characteristic exponent of the time-power-law is different, specifically 1/3 for diffusion-limited motion and 1/2 for attachment/detachment limited. By using Eqs. (4) and (5) to fit the experimentally determined $G(t)$ and $C(t)$, we can determine the exponent and calculate values of $C(0)$, τ_c and the pre-exponential factor of $G(t)$, which is denoted as G_0 in Eq. (4). The average value of the measured exponents is 0.23 ± 0.02. This clearly shows that the fluctuations of steps with C_{60} molecules are dominated by step-edge diffusion, the same as for the fluctuations of steps on bare Ag(111) surfaces. For more precise comparison of G_0, we then fix the exponent at 1/4 to determine the other parameters governing the correlation functions. In Fig. 5(a), the fit (solid blue line) shows the time correlation function scales very well as $t^{1/4}$ up to a length scale of $\sqrt{G(t_s)} \sim 0.3$ nm for the 51.0 nm step, where t_s is the saturation time, of order 5.0 s. Figure 5(b) shows the corresponding autocorrelation function and fitting curve, from which we can extract C(0) and τ_c. The results are shown in Fig. 6, in which we can see that τ_c does not show any obvious dependence on step lengths or step orientations. The simple average of the measured correlation times yields $\tau_c=10.6$ s. A linear fit yields a slope of 34 ± 56 ms/nm, indicating no significant functional dependence on step lengths. The observation that the correlation time is constant is consistent with previous studies where the correlation time was determined to be limited by the measurement time. In this case, the measured correlation time is equal to 1/9.7 times the measurement time, as also observed previously for steps without C_{60}.[1] Physically this result occurs when the measurement time limits the fluctuation wavelengths that are sampled within the measurement.[14]

Although the correlation time is constant, G_0 depends strongly on step orientations, with values for steps along the close-packed directions consistently smaller than those of misoriented steps. Since G_0 represents the magnitude of step fluctuations, this indicates that fluctuations of steps

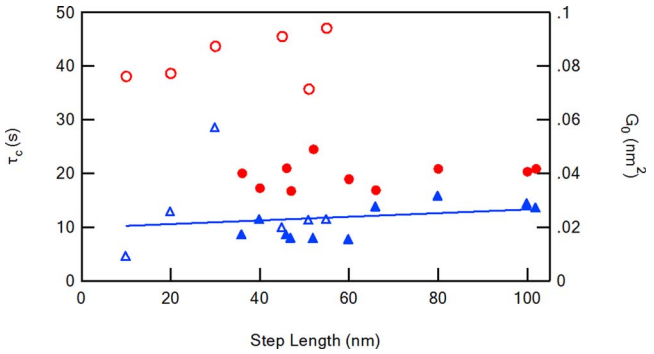

FIG. 6. (Color online) G_0 (right axis) and τ_c (left axis) vs step lengths l_{step}. Circles (red), G_0, with solid circles for close-packed steps and open circles for misorientated steps. Triangles (blue), τ_c, with solid triangles for close-packed steps and open triangles for misorientated steps. The angles for steps deviating from close-packed direction were: $l_{\text{step}}=10$ nm, $\theta=8°$; $l_{\text{step}}=20$ nm, $\theta=26°$; $l_{\text{step}}=30$ nm, $\theta=7°$; $l_{\text{step}}=45$ nm, $\theta=14°$; $l_{\text{step}}=51$ nm, $\theta=5°$; and $l_{\text{step}}=55$ nm, $\theta=17°$. Solid line (blue), linear fit for τ_c.

along close-packed directions (which we denote as step angle $\theta=0°$) are smaller than fluctuations of steps along low-symmetry directions. A possible explanation is the orientational variation of the step stiffness.[15] Close-packed steps are expected to be stiffer than misorientated steps. Another possible contribution to this orientation dependence of G_0 is the step mobility.

To evaluate the effective system size L from Eqs. (4)–(7), it is necessary to have a value for the step stiffness. Recently experimental and theoretical studies have shown that the Ag(111) step stiffness $\tilde{\beta}$ is a strongly varying function of the step orientation for small step angles at room temperature.[15–17] At room temperature, the thermal energy is roughly equivalent to $0.22\varepsilon_k$ (ε_k=the kink energy), and the exact form[18] for the step stiffness is well approximated by a remarkably simple equation:[15]

$$\frac{k_B T}{\tilde{\beta}(\theta) a_{\parallel}} = \frac{\sin(3\theta)}{2\sqrt{3}}, \tag{8}$$

The corresponding angular dependence of the stiffness is shown as the solid line in Fig. 7. The validity of this equation only breaks down for steps oriented very close to the high-symmetry direction ($|\theta|<2°$). Because these steps are experimentally very difficult to distinguish from high symmetry steps, their stiffness is most easily fit to the exact high-symmetry result:[15]

$$\frac{k_B T}{\tilde{\beta}(0) a_{\parallel}} = \frac{3(y-1)}{2y\sqrt{y^2-2y-3}}, \tag{9}$$

with $y=\sqrt{\frac{1+3z}{z(1-z)}}$ and $z=e^{-2\varepsilon_k/k_B T}$. This result is shown as the open circle at $\theta=0°$ in Fig. 7. Equation (9) represents the stiffness maximum, so it will generally over-estimate the experimental step stiffness. The exact solution for the full orientation dependence of $\tilde{\beta}(\theta)$ can be numerically evaluated and is shown as open circles in Fig. 7. Given the stiffness, it is immediately possible to calculate the step mobility from

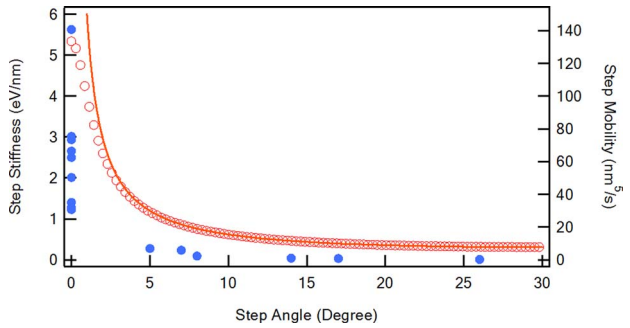

FIG. 7. (Color online) Step stiffness (left axis) and step mobility (right axis) vs step orientation. Solid line (red), low-temperature step stiffness as a function of the step angle [Eq. (8)]; open circle (red), exact step stiffness. Solid circles (blue), experimentally determined step mobility.

the measured values of G_0. The result is shown as (blue) solid circles in Fig. 7. The step mobility shows step orientation dependence similar to that of the step stiffness. For misoriented steps, covering an angular range $5°-26°$, the values of the step mobility are essentially constant, and much smaller than that of steps oriented along the close-packed direction. A large range of measured values of the step mobility for the nominally close-packed steps is likely because the step mobility is very sensitive to small changes in the angle. To quantify this observation, the hopping time for the fluctuations caused by the step diffusion can be expressed in terms of Γ_h, $a_{\parallel}$, and $a_{\perp}$: $\tau_h=a_{\perp}^2 a_{\parallel}^3/\Gamma_h$. Using the average of the measured values of Γ_n for close-packed steps and misoriented steps, we can roughly determine the corresponding hopping time. For close-packed steps, the hopping time constant is ~ 31 μs. For misoriented steps, the hopping time constant is ~ 704 μs, about twenty times larger than that of the close-packed steps.

Given the stiffness $\tilde{\beta}$, it is straightforward to calculate the values of the effective system size for steps with different lengths. Eliminating the mobility between Eqs. (4) and (7), the system size L can be expressed in terms of G_0, τ_c, $\tilde{\beta}$, and T:

$$L = \left(\frac{\pi^2 \tilde{\beta}}{k_B T \Gamma\left(\frac{3}{4}\right)} \right)^{\frac{1}{4}} \tau_c^{\frac{1}{4}} G_0. \tag{10}$$

The results are shown in Fig. 8. Using Eq. (6) to determine the system size, extracting L from the prefactor of the autocorrelation function C(0) [Eq. (6)], rather than from G_0 and τ_c, yields similar results providing a convenient consistency check. The ratios of the effective system size from Eqs. (6) and (10), L_6/L, are consistently near unity, with average value 1.17 ± 0.10. The dashed line in Fig. 8 shows the simplest expectation that L equals the step length. It is clear that the measured effective system sizes do not have a simple proportional dependence on the step length. In fact, there are two distinct regions, the first corresponding to close-packed steps (solid circles), and the second to misoriented steps (open circles). For both regions, the system sizes show at

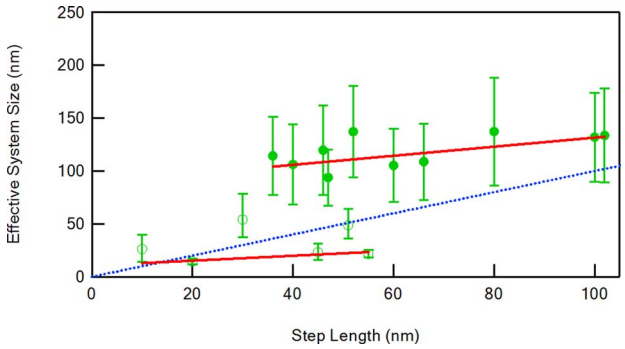

FIG. 8. (Color online) Measured effective system size vs step lengths. Circles (green), experimentally determined lengths with solid circles for steps orientated along close-packed direction and open circles for steps deviating from the close-packed direction. Dash line (blue), step lengths, $L=l_{\text{step}}$. Upper solid line (red), linear fit, $L=\text{a}+\text{b}\times l_{\text{step}}$, for the effective system size for the steps oriented along the close-packed direction with linear fit coefficients a=88 nm and b=0.42. Lower solid line (red), linear fit for the effective system size of the steps deviating from the close-packed direction with linear fit coefficients a=11 nm and b=0.23.

most weak dependence on the step lengths, with a slope of 0.42 ± 0.57 for close-packed steps, and slope 0.23 ± 0.13 for misoriented steps (solid lines in Fig. 8). The values of the effective length L of the close-packed steps are consistently longer than those of the misoriented steps, consistent with the different values of the stiffness. The effective system size for the close-packed steps is longer than the step length, indicating that the step length is not limiting the range of fluctuation wavelengths sampled in the measurement.

IV. DISCUSSION AND CONCLUSIONS

In summary, we have found that in C_{60} growth along step edges; $\langle 11\bar{2}\rangle$-orientated steps are the most adhesive for C_{60}, while step edges oriented along close-packed directions are less likely to bind C_{60}. The average value of the measured exponent for the correlation function $G(t)$, 0.23 ± 0.02 for steps of both orientation. This clearly shows the fluctuations of steps decorated with C_{60} molecules are dominated by step-edge diffusion just like clean steps. Our results further indicate for the step-edge diffusion case, the step mobility exhibits strong step orientation dependence. This is in contrast to the attachment-detachment dominated case on Ag(110), in which the step mobility does not depend appreciably on the step orientation.[19] In the standard Arrhenius model, the mobility Γ_h and hopping time τ_h are related to the attempt frequency ν and the effective activation barrier energy E_a^{eff}: $\Gamma_h \sim \frac{1}{\tau_h} = \nu e^{-E_a^{eff}/k_B T}$.[9,20] The effective activation energy incorporates the concentration of the diffusing species (the kink density) as well as the true energy barrier to diffusion. Considering the kink density, at the same temperature, the misoriented steps have higher kink density than that of the close-packed steps as demonstrated by the lower stiffness of the misoriented steps, and as expected based on statistical models.[21,22] Our result that the diffusion constant τ_h (mobility Γ_h) of the close-packed steps is lower (higher) than that of misoriented steps leads to the conclusion that the true activation energy for step-edge diffusion is lower on the close-packed step than the misoriented step. A strong dependence of diffusion rate on step-edge geometry is predicted for high-symmetry configurations,[23,24] although detailed calculations of continuous orientation dependence are not yet available. Developing an understanding of the orientational-dependence of the step mobility is important for understanding the evolution of thin film morphology under external driving forces.[25,26] The results for measured effective system sizes consistently show little dependence on the step lengths, but the effective system size does depend on the step orientations. As shown in Fig. 8, the measured correlation lengths are almost constants for the close-packed steps and the misoriented steps, respectively. The result is consistent with the expected behavior when the correlation times are limited by the measurement time. If a step edge has two pinning points at ends, the length of the step edge should determine the system size.[27] In our measurements, the step lengths between C_{60} sites range from 10 to ~100 nm. If the C_{60} molecules were real pinning points, the characteristic lengths would show step length dependence. Instead the measured correlation length for close-packed steps is consistently larger than the C_{60}-C_{60} separation, and the values of the length are consistent with fluctuations limited by the measurement time[1,14] for both high and low-symmetry step edges. Thus, the results indicate that C_{60} molecules are *not* acting as pinning points that prevent Ag migration on the step edges.

Previous studies of C_{60} on Au(111) and Ag(111) surfaces have revealed that the C_{60}-substrate interactions are considerable due to surface states.[3,28–30] For C_{60} on Ag(111), the adsorption energy is 1.5 eV. The interaction between C_{60} molecules and step edges is apparently stronger (enough to constrain C_{60} to step edges), in agreement with the observation that no individual stationary C_{60} molecules were on terraces at room temperature. Considering the geometry of step edges of (111) surfaces and C_{60}, the zigzag shape of steps along the $\langle 11\bar{2}\rangle$ direction provides a perfect match for the natural lattice constant of C_{60} molecules, which can thus align into close-packed chains along step edges. There is no detectable C_{60} motion once C_{60} molecules have connected into chains along the step edges, suggesting that the near-neighbor intermolecular attraction hinders C_{60} movement.

In our measurement time range, C_{60} molecules remain at fixed positions and show no scan-to-scan variability. However, the quantitative step fluctuation features indicate that C_{60} molecules are not acting as pinning points that would limit the correlation length of the step fluctuations. In order to understand why C_{60} molecules do not change step fluctuations, we need to consider not only the geometric effect of C_{60} molecules along the step edge, but also the local electron redistribution caused by C_{60} molecules. Both previous experimental and theoretical studies show that there is charge transfer from Ag(111) surfaces to C_{60} molecules.[20,21] The theoretical calculations provide further insight into the charge redistribution between Ag(111) surfaces and C_{60} molecules.[29] The interaction between C_{60} and the surface is primarily covalent, with some ionic character (0.5 electron

transfer per C_{60} molecule). The largest electron accumulation occurs in the middle of the interface region between the C_{60} and the top surface layer. The electron accumulation in the interface region corresponds to a strong local electric field, similar to that considered in Feibelman's analysis of surface diffusion on Pt(001).[31] Feibelman showed that when an external electric field is oriented to pull electrons out of the metal, Pt adatoms gain charge and become more like Au. As a result, their bonds to the surface weaken, and therefore the diffusion barrier diminishes. It is reasonable to expect that the charge redistribution caused by C_{60} should also change adatom diffusion along the step edges, possibly enhancing it enough to compensate for geometric effects. The geometric effects are illustrated in Fig. 9, using a simple lattice model with the value of 0.09 nm for the distance from the edge of C_{60} molecules to the underneath surface and the nearest step edge.[28] The resulting spacing shows that the maximum radius of adatoms that could hop through the gap between C_{60} and step edges is less than 0.1 nm, which is less than the radius of Ag atoms in the bulk, ~0.145 nm. This implies that Ag adatom diffusion could be constrained to substitutional motion or diffusion around the C_{60} molecules on the neighboring terraces. For both possibilities, the geometric effects would suggest hindered adatom movement along the step edges. Overall the geometric effect and the charge redistribution effect by C_{60} molecules may counteract each other. This, or perhaps more exotic explanations of correlated motion,[32] is needed to explain the unexpected result that the C_{60} atoms at the step edges provide little or no restriction to the fluctuations of intervening step-edge segments.

More succinctly, our results show that C_{60} molecules have no detectable effect on mass transfer along a defect structure (step edge) on the Ag(111) surface. This surprising conclusion opens the possibility that metal diffusion may also be facile under other electronegative organic molecules on metal surfaces.[33] If it proves general, this phenomenon will be significant in controlling nanometer-scale device fabrication, in which mass transport on metal electrodes plays a key role.

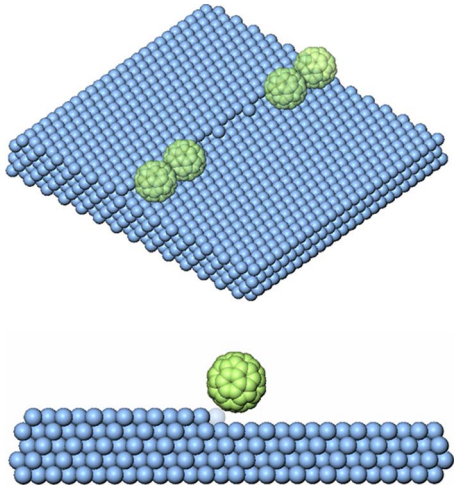

FIG. 9. (Color online) Schematic illustrations of the step with C_{60}. C_{60} molecules stay side by side to form chains along step edges, partly covering step edges.

ACKNOWLEDGMENTS

This work has been supported by the UMD NSF-MRSEC under Grant No. DMR 05-20471 and by the University of Maryland.

*Corresponding author. Email address: edw@umd.edu

[1] O. Bondarchuk, D. B. Dougherty, M. Degawa, E. D. Williams, M. Constantin, C. Dasgupta, and S. Das Sarma, Phys. Rev. B **71**, 045426 (2005).
[2] H.-C. Jeong and E. D. Williams, Surf. Sci. Rep. **34**, 171 (1999).
[3] E. I. Altman and R. J. Colton, Phys. Rev. B **48**, 18244 (1993).
[4] T. Sakurai, X. D. Wang, T. Hashizume, V. Yurov, H. Shinohara, and H. W. Pickering, Appl. Surf. Sci. **87-8**, 405 (1995).
[5] E. I. Altman and R. J. Colton, Surf. Sci. **295**, 13 (1993).
[6] X. Lu, M. Grobis, K. H. Khoo, S. G. Louie, and M. F. Crommie, Phys. Rev. Lett. **90**, 096802 (2003).
[7] M. Giesen, J. Frohn, M. Poensgen, J. F. Wolf, and H. Ibach, J. Vac. Sci. Technol. A **10**, 2597 (1992).
[8] L. Kuipers, M. S. Hoogeman, and J. W. M. Frenken, Phys. Rev. Lett. **71**, 3517 (1993).
[9] M. Giesen, Prog. Surf. Sci. **68**, 1 (2001).
[10] M. Giesen, C. Steimer, and H. Ibach, Surf. Sci. **471**, 80 (2001).
[11] C. Dasgupta, M. Constantin, S. Das Sarma, and S. N. Majumdar, Phys. Rev. E **69**, 022101 (2004).
[12] N. C. Bartelt, J. L. Goldberg, T. L. Einstein, E. D. Williams, J. C. Heyraud, and J. J. Metois, Phys. Rev. B **48**, 15453 (1993).
[13] N. C. Bartelt and R. M. Tromp, Phys. Rev. B **54**, 11731 (1996).
[14] D. B. Dougherty, C. Tao, O. Bondarchuk, W. G. Cullen, E. D. Williams, M. Constantin, C. Dasgupta, and S. Das Sarma, Phys. Rev. E **71**, 021602 (2005).
[15] T. J. Stasevich, H. Gebremariam, T. L. Einstein, M. Giesen, C. Steimer, and H. Ibach, Phys. Rev. B **71**, 245414 (2005).
[16] M. Ondrejcek, M. Rajappan, W. Swiech, and C. P. Flynn, Surf. Sci. **574**, 111 (2005).
[17] M. Ondrejcek, W. Swiech, M. Rajappan, and C. P. Flynn, Phys. Rev. B **72**, 085422 (2005).
[18] R. K. P. Zia, J. Stat. Phys. **45**, 801 (1986).
[19] W. W. Pai, N. C. Bartelt, and J. E. Reutt-Robey, Phys. Rev. B **53**, 15991 (1996).
[20] F. Szalma, D. B. Dougherty, M. Degawa, E. D. Williams, M. I. Haftel, and T. L. Einstein, Phys. Rev. B **73**, 115413 (2006).
[21] E. D. Williams and N. C. Bartelt, in *Handbook of Surface Science*, edited by W. N. Unertl (Elsevier: Amsterdam, 1996), Vol. 1, pp. 51–99.
[22] H. M. Cuppen, H. Meekes, E. Van Veenendaal, W. J. P. van Enckevort, P. Bennema, M. F. Reedijk, J. Arsic, and E. Vlieg, Surf. Sci. **506**, 183 (2002).
[23] S. Durukanoglu, A. Kara, and T. S. Rahman, Surf. Sci. **587**, 128 (2005).

[24] M. C. Marinica, C. Barreteau, D. Spanjaard, and M.-C. Desjonquères, Phys. Rev. B **72**, 115402 (2005).
[25] J. Cho, M. Rauf Gungor, and D. Maroudas, Appl. Phys. Lett. **85**, 2214 (2004).
[26] P. Kuhn, J. Krug, F. Hausser, and A. Voigt, Phys. Rev. Lett. **94**, 166105 (2005).
[27] A. Pimpinelli, J. Villain, D. E. Wolf, J. J. Metois, J. C. Heyraud, I. Elkinani, and G. Uimin, Surf. Sci. **295**, 143 (1993).
[28] L. L. Wang and H. P. Cheng, Phys. Rev. B **69**, 045404 (2004).
[29] L. L. Wang and H. P. Cheng, Phys. Rev. B **69**, 165417 (2004).
[30] A. Fartash, Phys. Rev. B **52**, 7883 (1995).
[31] P. J. Feibelman, Phys. Rev. B **64**, 125403 (2001).
[32] P. J. Feibelman, Surf. Sci. **478**, L349 (2001).
[33] Q. Guo, X. Sun, and R. E. Palmer, Phys. Rev. B **71**, 035406 (2005).